Philosophical Magazine

ISSN: 0031-8086 (Print) (Online) Journal homepage: www.tandfonline.com/journals/tphm19

A chemical diffusion model for partitioning of transition elements in oxide scales on alloys

M. G. C. Cox, B. Mcenaney & V. D. Scott

To cite this article: M. G. C. Cox, B. Mcenaney & V. D. Scott (1972) A chemical diffusion model for partitioning of transition elements in oxide scales on alloys, Philosophical Magazine, 26:4, 839-851, DOI: 10.1080/14786437208226960

To link to this article: https://doi.org/10.1080/14786437208226960

Published online: 02 Sep 2006.

A Chemical Diffusion Model for Partitioning of Transition Elements in Oxide Scales on Alloys

By M. G. C. Cox, B. McEnaney, and V. D. Scott
School of Materials Science, University of Bath, U.K.

[Received 1 May 1972 and after revision 25 May 1972]

Abstract

A mechanism based on lattice diffusion of cations is proposed to account for segregation of transition elements in scales on oxidized ferrous alloys. From considerations of diffusion paths through close-packed oxide lattices, the mobility of a cation is related to the difference in stabilization energies for octahedral and for tetrahedral sites, as estimated from crystal field theory. The proposed correlation between crystal field preference energy and cation mobility is substantiated by reference to experimental oxidation rates for certain transition elements. The ranking order established for ease of diffusion of cations through close-packed oxide lattices is then shown to agree with the measured distribution of elements in scales formed on iron-chromium alloys by oxidation at 600°C in CO_2-based gas. The model also accords with previously published data on partitioning in oxides.

§ 1. Introduction

The formation of duplex scales on oxidized ferrous alloys, accompanied by segregation of the alloying elements, has been reported frequently in the literature. Pfeil (1929) showed that most of the transition elements, with the exception of manganese, were concentrated within the inner layer of oxide formed on alloy steels in air at 1000°C. The findings have since been substantiated and extended by a large number of workers. For example, Brenner (1955) found molybdenum concentrated in the inner scale on iron–molybdenum alloy oxidized at 1000°C. Moreau (1953) reported a similar effect on iron–chromium alloys and Rahmel (1962) found that vanadium, chromium, silicon and molybdenum were confined to the inner oxide scale of the respective binary iron alloys oxidized at 1000°C in oxygen. Similar partitioning behaviour has been observed on more complex iron alloys, both ferritic and austenitic, and also in a variety of oxidizing environments. In work comparable with the present study, Antill, Peakall and Warburton (1968) noted duplex scales on steels oxidized in CO_2 gas in which the inner oxide contained chromium and molybdenum while iron and manganese were distributed throughout the double layer.

Despite the large accumulation of data on segregation effects in oxide layers, there appears to have been little attempt to explain this behaviour, apart from Surman and Castle (1969) who invoked a vapour phase transport mechanism to account for segregation of chromium in the inner layer of

oxide. This paper describes the characterization of oxide scale structures formed on iron–chromium alloys by oxidation at 600°C in CO_2-based gas and relates the findings to kinetic data. A model based on lattice diffusion of cations is then proposed to explain the observed segregation of chromium in the duplex scale. The mechanism is shown to have greater general application to the oxidation of transition metals and their alloys than any previous approach.

§ 2. Experimental Details

2.1. *Oxidation Experiments*

2.1.1. *Apparatus*

The apparatus, constructed to study the oxidation of iron–chromium alloys in CO_2-based gas at atmospheric pressure in the temperature range 400°–600°C, consisted of two vertically mounted reaction tubes, each surrounded by a furnace controlled to ± 2°C. The kinetics of the oxidation were followed gravimetrically on a specimen suspended from a sensitive microbalance and contained in one of the reaction tubes ; samples for microstructural analysis were produced simultaneously in the second reaction tube. A common gas supply in the systems ensured that gravimetric and microstructural experiments were carried out under identical conditions.

The oxidation studies described here were conducted at 600°C for periods of up to 100 hours in a flowing gas of CO_2–1% CO.

2.1.2. *Materials*

Binary iron alloys containing 5, 9, 12 and 20% chromium were prepared by vacuum melting followed by cold rolling with interstage anneals. Major impurities present in the iron and chromium starting materials are listed in table 1.

Table 1. Impurity levels (p.p.m.) in iron and chromium starting materials

	C	N	S	P	Mn	O
Carbonyl iron	< 200	< 200	< 30	< 15	< 100	low
Grade 1 chromium	< 50	< 20				< 120

The sheet specimens approximately 50 × 10 × 1 mm were first degreased and then chemically polished in a hot aqueous solution containing 15% hydrochloric acid, 10% hydrofluoric acid and 30% nitric acid to remove any surface contamination. After annealing in dry hydrogen at 1000°C to eliminate any cold-worked structure, they were given a further chemical polish.

2.1.3. *Procedure*

After introducing specimens into the reaction tubes, the apparatus was evacuated to $< 10^{-4}$ Torr. The specimens were then raised to temperature,

the gas admitted (linear flow rate $1{\cdot}3\,\mathrm{mm\,sec^{-1}}$) and the weight gain followed on the microbalance. After completion of an oxidation experiment the specimen suspended from the microbalance was cooled rapidly by lowering the furnace with gas flowing, while samples for microstructural analysis were removed as required through an air-lock device.

2.2. *Microstructural Analysis*

Surface topography of the oxidized metal was studied by scanning electron microscopy. This was complemented by reflection electron diffraction and x-ray diffraction to identify crystal structures in the surface regions of the oxide. The outer oxide was stripped from the specimen for more detailed analysis, at the same time allowing access of x-rays to the inner layer for structural identification.

Sections through the oxidized metal were prepared by metallographic polishing followed by etching when required, both being carefully controlled to minimize distortion of surface features. In addition to optical and scanning electron microscopy, electron probe microanalysis was carried out on polished sections to determine distributions of elements in the scale. Sections through the oxidized metal devoid of polishing artefacts were produced by inducing brittle fracture after cooling in liquid nitrogen and these were also examined in the scanning electron microscope.

§ 3. Experimental Results

The oxidation kinetics of the 5% chromium alloy at 600°C are characterized by a linear oxidation rate for the first few hours followed by a parabolic rate until completion of the experiment, ca.100 hours. The parabolic rate constant was found to be $1{\cdot}2 \times 10^{-8}\,\mathrm{kg^2\,m^{-4}\,sec^{-1}}$ (table 2).

Table 2. Data for oxidation of Fe–Cr binary alloys in CO_2–1% gas at 600°C

Cr in alloy (wt %)	Rate constant, k ($\mathrm{kg^2\,m^{-4}\,sec^{-1}} \times 10^8$) $\pm 0{\cdot}3$	Spinel formula for inner oxide	Ratio of Cr in spinel to Cr in metal, f_2/f_1 ($\pm 0{\cdot}1$)
5	1·2	$Fe(Fe_{1\cdot7}Cr_{0\cdot3})O_4$	1·5
9	0·9	$Fe(Fe_{1\cdot4}Cr_{0\cdot6})O_4$	1·5
12	0·7	$Fe(Fe_{1\cdot2}Cr_{0\cdot8})O_4$	1·5
20	1·2	$Fe(Fe_{0\cdot7}Cr_{1\cdot3})O_4$	1·5

Scanning electron microscopy showed that the outer surface of the oxide consisted of faceted crystals, fig. 1, while a metallographically prepared section, fig. 2, clearly reveals that a duplex oxide scale has been formed ; the ratio of thicknesses of outer and inner oxide, R, is

Fig. 1

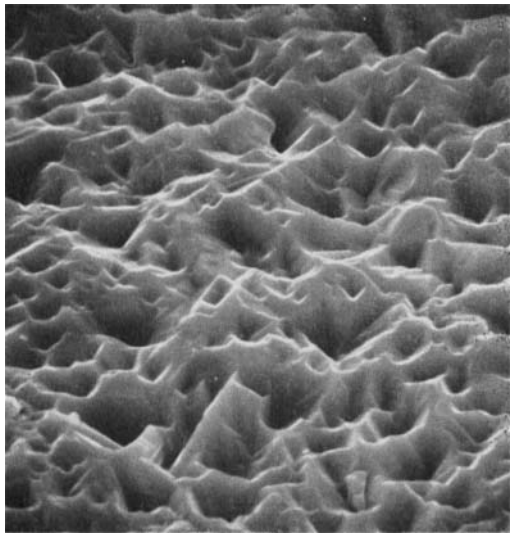

Fe–5% Cr alloy oxidized at 600°C. Outer surface. Scanning electron micrograph × 3500.

Fig. 2

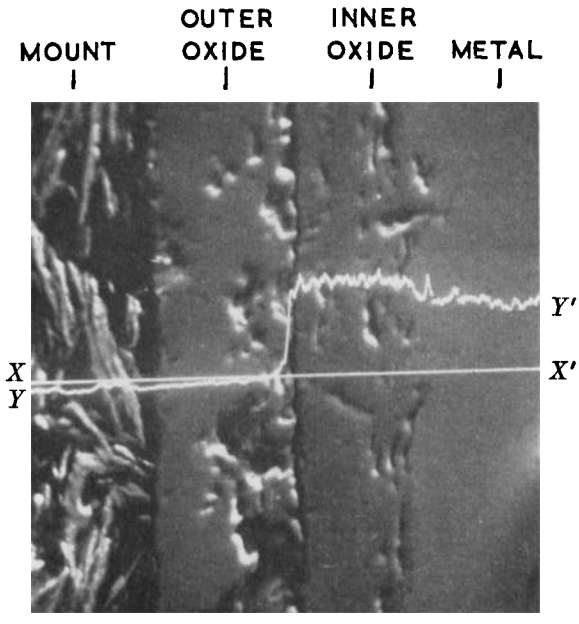

As fig. 1. Polished section showing duplex nature of oxide. Scanning electron micrograph × 600. Chromium concentration YY' measured along the line XX', showing negligible chromium in the outer oxide, is superimposed.

approximately unity. A plot of chromium concentration, YY', across the double layer along the line XX', has been superimposed on fig. 2. These data, obtained using the electron probe microanalysis attachment to the microscope, were supplemented with information obtained with a conventional microanalyser, fig. 3. The chromium level in the inner oxide is approximately 1·5 times its concentration in the metal and

Fig. 3

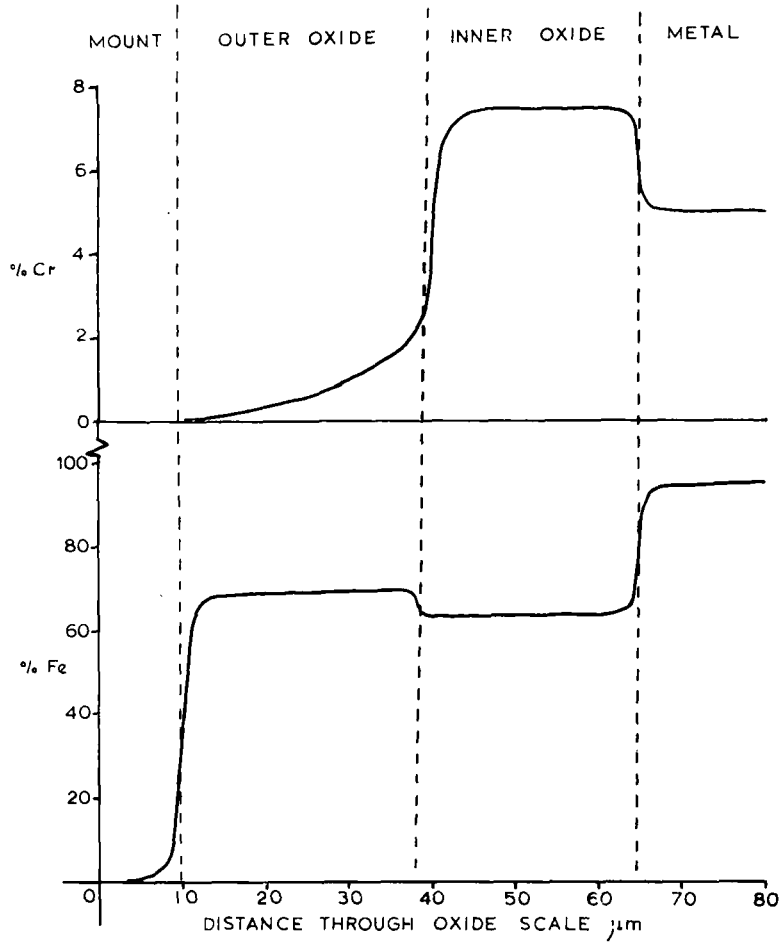

As fig. 2. Microanalysis plots of metal concentration versus distance.

decreases sharply at the oxide–oxide interface to an undetectable amount in the outer surface regions; part of the 'tail' in the outer oxide is due to fluorescence uncertainty (Reed and Long 1963) and the actual concentration gradient at the oxide–oxide interface may well be steeper than indicated. Diffraction studies on both attached and detached oxide layers showed that the inner and outer oxides possessed a spinel type of crystal structure.

The outer layer was thus concluded to be magnetite, Fe_3O_4, while the inner chromium-containing spinel was best represented by $Fe(Fe_{1.7}Cr_{0.3})O_4$.

A typical scanning electron micrograph from a fractured specimen, fig. 4, shows vestiges of polishing scratches on the outer surface of the inner oxide, indicating that it was formed from the original metal surface.

Fig. 4

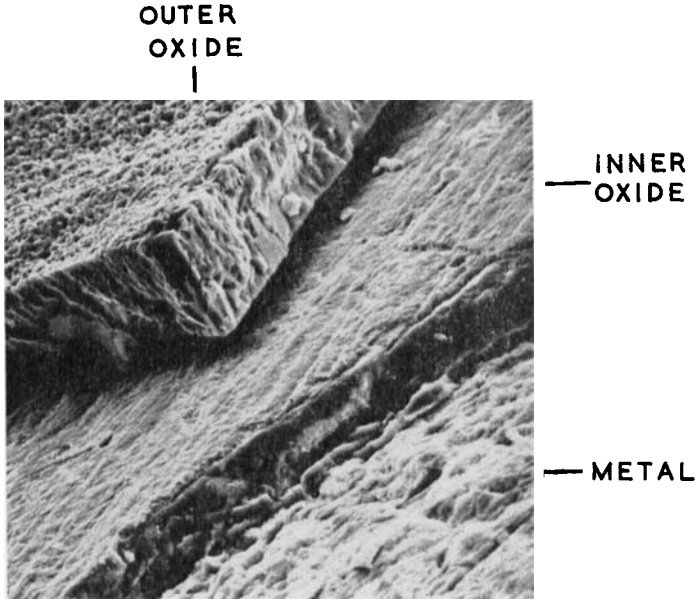

As fig. 1. Fracture section showing clearly the two oxide layers and the metal substrate. Scanning electron micrograph $\times 350$.

The oxidation behaviour of the 9, 12 and 20% chromium alloys was very similar to that of the 5% alloy. Duplex oxide layers with spinel structures were formed with thickness ratios, R, of approximately one. The parabolic rate constants and formulae for the inner spinels are given in table 2, the outer layers being essentially magnetite in each case. Variation in the chromium content of the alloys does not appear to affect the rate constant significantly, a typical series of repeat measurements on an alloy giving values ranging from 0·7 to $1{\cdot}2 \times 10^{-8} kg^2 m^{-4} sec^{-1}$.

§ 4. Discussion

The model presented in this paper to account for the partitioning of transition elements in duplex scales on oxidized alloys is developed by considering the paths available to cations for lattice diffusion in close-packed oxides. The energetics of cation transfer through the lattice are related to cation site preference energies, calculated for first row transition elements from crystal field theory. This leads to ranking orders for cationic

mobility which are shown to be in accord with experimental data on the oxidation kinetics of first row transition metals and on the segregation of elements in duplex scales.

4.1. *The Oxidation Process*

In the case of the iron–chromium alloys examined in the present work a linear oxidation rate of short duration, presumably associated with an interface reaction, is followed by a parabolic oxidation rate characteristic of a diffusion controlled process. Since markings on the unoxidized metal surface were subsequently located at the oxide–oxide interface, fig. 4, the outer oxide layer must have grown by outward movement of iron-containing species, an interpretation consistent with the unconstrained growth morphology of oxide crystals observed at the oxide–gas interface.

As oxidation proceeds, the thickness ratio of the inner and outer layers of oxide approaches unity, in accord with the above mechanism as the following analysis shows.

If the total weight of metal oxidized is W, then the volume of the vacated space below the original metal surface due to the outward diffusion of metal may be written as W/ρ_m and the weight of the inner oxide which fills that space as $W\rho_o/\rho_m$, where ρ_m and ρ_o are the densities of the metal and oxide, respectively. Putting f equal to the weight fraction of metal in the oxide, the weight of metal in the inner oxide will be $Wf\rho_o/\rho_m$ and in the outer oxide, $W(1-f\rho_o/\rho_m)$. Thus the volume of the outer oxide is $W(1-f\rho_o)\rho_m)/\rho_o f$, and the ratio of thicknesses of the inner to the outer oxides, R, may be written $R=f\rho_o/(\rho_m-f\rho_o)$.

Taking $\rho_m=7{\cdot}8$ g/ml and $\rho_o=5{\cdot}2$ g/ml and $f=0{\cdot}72$ for a spinel $Fe(Fe_{2-x}Cr_x)O_4$, the thickness ratio R is 0·93, which is close to the experimentally determined value.

Further, for an alloy containing a chromium weight fraction f_1, the weight of chromium oxidized is Wf_1. The weight of inner oxide is $W\rho_o/\rho_m$ and, assuming that the chromium is retained in the inner layer, the weight fraction of chromium in this layer, f_2, is given by

$$f_2=\frac{Wf_1}{W\rho_o/\rho_m}=f_1\rho_m/\rho_o=1{\cdot}5f_1$$

This figure is in agreement with findings in the present work (table 2).

Thus as the outer oxide grows by outward movement of metal, the inner oxide grows to fill the vacated space, from which it follows that outward movement of metal through the outer layer is the rate-controlling process. It is here proposed that the mechanism of outward transport in the oxide is by lattice diffusion of cations. Possible mechanisms for transport of oxygen through the inner layer have been discussed by Dravnieks and McDonald (1948) but, since these are not rate-controlling, they need not be considered further for the present analysis.

4.2. *The Lattice Diffusion Model*

Most oxide lattices relevant to the present work, including spinels, may be regarded as close-packed arrangements of oxygen anions containing cations in octahedral or tetrahedral interstices. Only a fraction of the available interstices are normally occupied, for example, only one quarter of the sites are filled in an AB_2O_4 spinel, and cation diffusion through the lattice may therefore occur via these unoccupied interstices.

Azaroff (1961) has considered possible diffusion paths for cations in close-packed anion lattices and the preferred route in cubic structures was shown to be via alternate, adjacent octahedral and tetrahedral positions, termed the Azaroff mechanism in this paper, while diffusion via similar interstices, i.e. tetrahedral to tetrahedral or octahedral to octahedral, is prohibited by the severe lattice distortion involved in these modes of cation transfer.

The rate of lattice diffusion of a cation through a close-packed oxide may be related to the activation energy for transfer from one type of interstice to the other, see fig. 5. The maximum strain energy of the system during the transfer, E_s, is associated with the passage of the cation between the trigonal arrangement of anions separating the two types of interstice. The energy difference between a cation placed in a tetrahedral field and in

Fig. 5

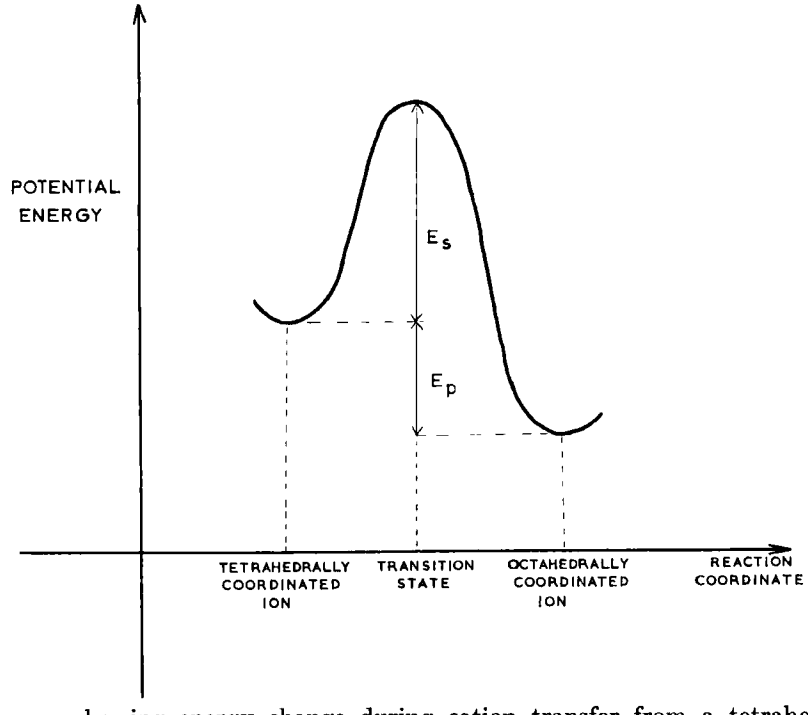

Diagram showing energy change during cation transfer from a tetrahedral site to an octahedral site in a close packed oxide.

an actahedral field, E_p, is shown in fig. 5 as an octahedral site preference energy, i.e. transfers from octahedral to tetrahedral positions will be more difficult than cation movement in the opposite sense. Thus diffusion of cations along the chains of octahedral and tetrahedral interstices may be related to the magnitude of E_p, i.e. the rate of diffusion of cations decreases with increase in E_p. Furthermore, since E_p is contained in the exponent of the Arrhenius equation relating diffusion coefficient D with temperature,

$$D = D_0 \exp[-(E_s + E_p)/RT],$$

small differences in E_p may have a large effect on diffusion rates.

For transition metal oxides the energy term E_p may be related to the difference in crystal field stabilization energy of the two types of interstice. The difference between the octahedral and tetrahedral crystal field stabilization energies for oxides, termed the crystal field preference energy (CFPE) in this paper, has been calculated from spectroscopic data by Dunitz and Orgel (1957) and is given in table 3.

Table 3. Crystal field preference energies (CFPE) for transition metal ions in oxides (from Dunitz and Orgel 1957)

Ion	Number of *d*-electrons	CFPE (kJ mol^{-1})
Ti^{3+}	1	29
V^{3+}	2	54
Cr^{3+}	3	158
Mn^{3+}	4	96
Mn^{2+}, Fe^{3+}	5	0
Fe^{2+}	6	17
Co^{2+}	7	31
Ni^{2+}	8	86
Cu^{2+}	9	64

In order of increasing crystal field preference energy, the series may thus be written :

for trivalent ions $Fe^{3+} : Ti^{3+} : V^{3+} : Mn^{3+} : Cr^{3+}$,
and for divalent ions $Mn^{2+} : Fe^{2+} : Co^{2+} : Cu^{2+} : Ni^{2+}$.

This would correspond to the predicted order for decreasing cation mobility through close-packed oxide lattices via the Azaroff mechanism.

4.3. *Evaluation of the Proposed Model*

Data on self-diffusion of cations in close-packed oxides are not sufficiently reliable to assess critically the proposed model but, since in many cases lattice diffusion of cations controls rates of oxidation of pure metals (Kubaschewski and Hopkins 1967), the latter may be used for this purpose. In such cases the variation of oxidation rate with temperature may be written in terms of the rate constant k,

$$\log k = \log k_0 - E_s/_{2{\cdot}303RT} - E_p/_{2{\cdot}303RT}.$$

Fig. 6

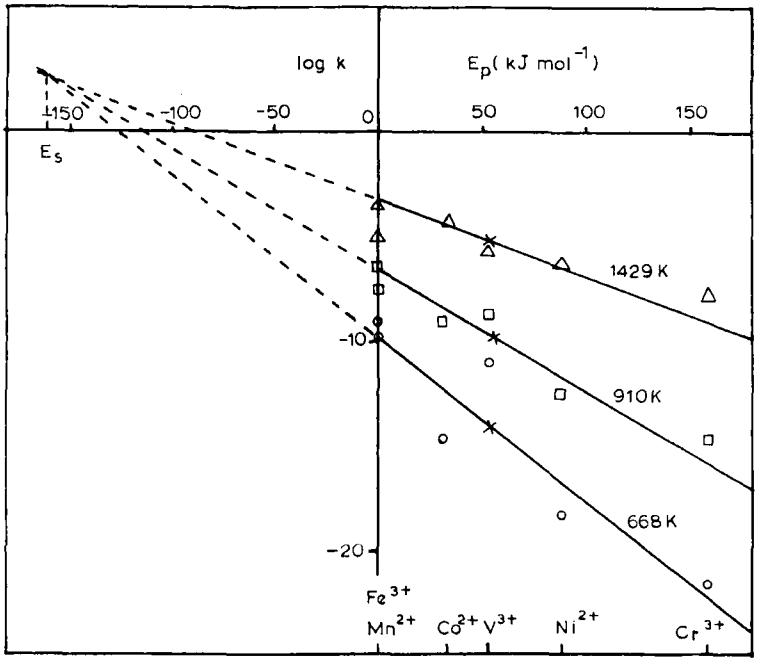

Plot of log k versus E_p for Fe, Mn, Co, V, Ni, Cr at 668 K, ○, 910 K, □, and 1429 △. The lines are of slope $1/2{\cdot}303RT$ passing through the centroid, X.

In fig. 6 log k is plotted against E_p for first row transition elements. The oxides of the metals used here have close-packed cubic anion lattices, except Cr_2O_3 where the anions are situated on a hexagonal sublattice. Azaroff (1961) has shown that in the hexagonal structure adjacent octahedral interstices parallel to the c-axis form possible diffusion paths. However, two-thirds of these positions in Cr_2O_3 will be already occupied by cations and either the diffusing cation will have to by-pass the occupied site by way of a tetrahedral interstice or the occupying cation must be displaced to a tetrahedral position to create an octahedral vacancy. These two processes are energetically equivalent and in both cases the rate of transfer of the cation is determined by the difference in energy when placed in an octahedral and a tetrahedral position as in cubic close-packed structures. High-temperature oxidation data ($T > 1000$ K) have been used in fig. 6 wherever possible since at lower temperatures ($T <$ ca. 800 K) grain-boundary diffusion may be important. Titanium and copper are omitted from fig. 6, since the former oxidises by inward diffusion of anions (Kubaschewski and Hopkins 1967) and neither titanium nor copper forms close-packed oxides.

In the case of vanadium, volatility of the pentoxide precludes quantitative measurements of oxidation rates at high temperatures and, consequently, low-temperature results ($T < 873$ K) were used.

The points in fig. 6 lie close to straight lines of slope $1/2{\cdot}203\,RT$, which indicates to a first approximation that the variation of E_s through the series is small compared with variations in E_p. It should also be noted that the magnitude of the strain energy term E_s, estimated from the intersection as 159 kJ mol^{-1}, is of the same order of magnitude as some of the octahedral site preference energies, E_p, given in table 3.

The observed scatter of points about the straight line may be attributed to a number of factors. For example, since trivalent cations are smaller than divalent cations they will pass more easily between the trigonal arrangement of anions which separate one type of interstice from the other and result in a smaller value of E_s : this effect is most clearly seen in the positions of Fe^{3+} and Mn^{2+} in fig. 6 where, for $E_p = 0$, E_s is smaller for the trivalent ion. In the case of the rocksalt structures of CoO and NiO, all the octahedral sites are filled and vacancies may have to be created before appreciable cation diffusion can occur, adding an extra energy term to the activation energy, E_A, for oxidation of those elements. For vanadium, the activation energy for oxidation is lower than that predicted from crystal field preference energy, possibly due to a significant contribution from grain-boundary diffusion to the low-temperature oxidation rate data used in this case.

The correlation thus established between parabolic oxidation rate and crystal field preference energy for a number of first row transition elements leads to the following conclusions: (i) oxidation of these elements is controlled by lattice diffusion of cations through the oxide ; and (ii) rate of diffusion of cations is determined principally by crystal field preference energy.

4.4. *Application of the Model to Segregation of Elements in Oxide Scales on Alloys*

The virtual absence of chromium from the outer oxide on iron–chromium alloys oxidized at 600°C is in accord with the above hypothesis that the Cr^{3+} ion will diffuse with difficulty through spinel oxides. In addition the oxidation results of Pfeil (1929), which indicate that the first row transition elements may be placed in the following order of decreasing cation mobility, Fe : Mn : V : Ni : Cr, are substantially in agreement with principles presented in this paper. It follows that as cationic mobility increases with increase in oxidation temperature, partitioning effects will be less marked, which would account for the steeper concentration gradient at the oxide–oxide interface found in the present work compared with Pfeil's work on iron–chromium alloys oxidized at 1000°C. The presence in the outer oxide of only iron and manganese among the first row transition elements is in accord with the lack of crystal field preference energy calculated for Fe^{3+} and Mn^{2+}. In the case of Fe_3O_4 scales, the transfer of Fe^{2+} can also occur due to the ready interconversion of Fe^{2+} and Fe^{3+} by an electron hopping mechanism (Robbins, Wertheim, Sherwood and Buchanan 1971).

It is considered that the cation diffusion model has more general application than the mechanism of Surman and Castle (1969) where transport by volatile $Fe(OH)_2$ was proposed to account for segregation in scales on iron–chromium alloys oxidized on steam at 400°–500°C, chromium remaining in the inner layer because it forms no such volatile compound. Surman and Castle discounted any contribution by cation or anion diffusion to the oxidation rate from a comparison of experimental kinetic data with calculations for various transport mechanisms. However, had grain-boundary effects been taken into account by using an activation energy for cation diffusion approximately one half the assumed value of 230 kJ mol^{-1} for lattice diffusion, their experimental results could be explained without invoking vapour phase transport.

The thickness ratio of the inner and outer oxide layers found for the iron–chromium alloys examined in the present work is consistent with rate control by cationic diffusion through the outer magnetite layer and, since the same outer oxide structure was found for all alloy compositions, their similar oxidation rate constants may be explained. The virtual lack of dependence of oxidation rate on chromium content would also be expected from the hypothesis, as replacement of Fe^{3+} by Cr^{3+} in the spinel oxide would not significantly alter the number of unoccupied sites or the activation energy for iron cation movement. The observation is in contrast with the minimum rate found for oxidation of iron–20% chromium alloy at 600°–900°C in oxygen at atmospheric pressure, which was at least an order of magnitude less than for the 10 and 30% binary alloys (Footner, Holmes and Mortimer 1967). However, in the latter work solid solutions of rhombohedral oxides were formed on the alloys from *n*-type (Fe_2O_3) and *p*-type (Cr_2O_3) structures, with a minimum defect concentration in the oxide on the 20% chromium alloy which could be related to the minimum oxidation rate.

The principles described in this paper are in accord with the partitioning behaviour observed on alloys of iron more complex than binary systems and, furthermore, data on non-ferrous alloys are also in agreement with the model. For example, the concentration of nickel in a duplex oxide scale on cobalt–nickel alloys is greater in the inner layer (Kubaschewski and Hopkins 1967). Clearly, application of these principles may be extended in an attempt to elucidate the oxidation behaviour of a wide range of alloys and the treatment may be refined to take into account polarization and electrostatic contributions to cationic site preference energies in close-packed oxides (Miller 1959).

Acknowledgments

The authors wish to thank Professor F. S. Stone and Mr. W. H. Whitlow for helpful discussions and the C.E.G.B. for permission to publish this paper.

References

Antill, J. E., Peakall, K. A., and Warburton, J. B., 1968, *Corros. Sci.*, **8,** 689.

Azaroff, L. V., 1961, *J. appl. Phys.*, **32,** 1638.

Brenner, S. S., 1955, *J. electrochem. Soc.*, **102,** 7.

Dravnieks, A., and McDonald, H. J., 1948, *J. electrochem. Soc.*, **94,** 139.

Dunitz, J. B., and Orgel, L. E., 1957, *J. Phys. Chem. Solids*, **3,** 20 and 318.

Footner, P. K., Holmes, D. R., and Mortimer, D., 1967, *Nature, Lond.*, **216,** 54.

Kubachewski, O., and Hopkins, B. E., 1967, *Oxidation of Metals and Alloys*, (Butterworths).

Miller, A., 1959, *J. appl. Phys.*, Suppl., **30,** 245.

Moreau, J., 1953, *Comptes Rendus*, **236,** 85.

Pfeil, L. B., 1929, *J. Iron Steel Inst.*, **119,** 501.

Rahmel, A., 1962, *Z. Elektrochem.*, **66,** 363.

Reed, S. J. B., and Long, J. V. P., 1963, *X-ray Optics and Microanalysis*, edited by H. E. Pattee, V. E. Cosslett and A. Engstrom, Vol. 3 (New York : Academic Press), p. 317.

Robbins, M. G., Wertheim, G. K., Sherwood, R. C., and Buchanan, D. N. E., 1971, *J. Phys. Chem. Solids*, **32,** 717.

Surman, P. L., and Castle, J. E., 1969, *Corros. Sci.*, **9,** 771.